THE JOURNAL OF BIOLOGICAL CHEMISTRY VOL. 288, NO. 14, pp. 10176–10187, April 5, 2013

Rheb (Ras Homologue Enriched in Brain)-dependent Mammalian Target of Rapamycin Complex 1 (mTORC1) Activation Becomes Indispensable for Cardiac Hypertrophic Growth after Early Postnatal Period*

Received for publication, September 28, 2012, and in revised form, February 19, 2013 Published, JBC Papers in Press, February 20, 2013, DOI 10.1074/jbc.M112.423640

Takahito Tamai[‡], Osamu Yamaguchi[‡], Shungo Hikoso[‡], Toshihiro Takeda[‡], Manabu Taneike[‡§], Takafumi Oka[‡], Jota Oyabu[‡], Tomokazu Murakawa[‡], Hiroyuki Nakayama[¶], Yoshihiro Uno[‖], Kyoji Horie[**], Kazuhiko Nishida[‡§], Nahum Sonenberg[‡‡], Ajay M. Shah[§], Junji Takeda[**], Issei Komuro[‡], and Kinya Otsu[‡§1]

*From the [‡]Department of Cardiovascular Medicine, Graduate School of Medicine, Osaka University, Suita, Osaka 565-0871, Japan, the [§]Cardiovascular Division, King's College London British Heart Foundation Centre, London SE5 9NU, United Kingdom, the [¶]Department of Clinical Pharmacology and Pharmacogenomics, Graduate School of Pharmaceutical Sciences, [‖]Laboratory of Reproductive Engineering, The Institute of Experimental Animal Sciences, and **Department of Social and Environmental Medicine, Graduate School of Medicine, Osaka University, Suita, Osaka 565-0871, Japan, and the [‡‡]Department of Biochemistry and McGill Cancer Centre, McGill University, Montreal, Quebec H3G 1Y6, Canada*

Background: Rheb (Ras homologue enriched in brain) regulates mammalian target of rapamycin complex 1 (mTORC1).
Results: mTORC1 activity and cardiac hypertrophy are attenuated in Rheb-deficient hearts after the early postnatal period.
Conclusion: Rheb-dependent mTORC1 activation becomes essential for cardiomyocyte hypertrophic growth after the early postnatal period.
Significance: The findings provide insight into the regulatory mechanism of mTORC1 in postnatal heart development.

Cardiomyocytes proliferate during fetal life but lose their ability to proliferate soon after birth and further increases in cardiac mass are achieved through an increase in cell size or hypertrophy. Mammalian target of rapamycin complex 1 (mTORC1) is critical for cell growth and proliferation. Rheb (Ras homologue enriched in brain) is one of the most important upstream regulators of mTORC1. Here, we attempted to clarify the role of Rheb in the heart using cardiac-specific Rheb-deficient mice (*Rheb*$^{-/-}$). *Rheb*$^{-/-}$ mice died from postnatal day 8 to 10. The heart-to-body weight ratio, an index of cardiomyocyte hypertrophy, in *Rheb*$^{-/-}$ was lower than that in the control (*Rheb*$^{+/+}$) at postnatal day 8. The cell surface area of cardiomyocytes isolated from the mouse hearts increased from postnatal days 5 to 8 in *Rheb*$^{+/+}$ mice but not in *Rheb*$^{-/-}$ mice. Ultrastructural analysis indicated that sarcomere maturation was impaired in *Rheb*$^{-/-}$ hearts during the neonatal period. *Rheb*$^{-/-}$ hearts exhibited no difference in the phosphorylation level of S6 or 4E-BP1, downstream of mTORC1 at postnatal day 3 but showed attenuation at postnatal day 5 or 8 compared with the control. Polysome analysis revealed that the mRNA translation activity decreased in *Rheb*$^{-/-}$ hearts at postnatal day 8. Furthermore, ablation of eukaryotic initiation factor 4E-binding protein 1 in *Rheb*$^{-/-}$ mice improved mRNA translation, cardiac hypertrophic growth, sarcomere maturation, and survival. Thus, Rheb-dependent mTORC1 activation becomes essential for cardiomyocyte hypertrophic growth after early postnatal period.

Growth of the heart during embryonic development occurs primarily through proliferation of cardiac myocytes. However, cardiac myocytes withdraw from the cell cycle soon after birth and further increases in cardiac mass are achieved predominantly through hypertrophic growth rather than proliferation of individual myocytes (1). Normal heart development in perinatal period requires cardiomyocyte maturation, proliferation, and hypertrophy. However, the precise molecular mechanisms underlying perinatal cardiac development remain to be elucidated. The serine/threonine protein kinase Akt is an important mediator of phosphatidylinositol-3 kinase signaling and involved in postnatal cardiac growth (2). The stimulation of Akt signaling pathway leads to the activation of a master regulator of cell growth and metabolism, mammalian target of rapamycin complex 1 (mTORC1).[2] mTORC1 consists of five components, including mTOR, the Raptor (regulatory associated protein of mTOR), and PRAS40 (proline-rich Akt substrate 40 kDa) (3). One of the most important signaling molecules in the regulation of mTORC1 is the Ras homologue enriched in brain gene (*Rheb*). Rheb is ubiquitouly expressed in mammalian cells with the highest levels in skeletal and cardiac muscle (4). The *Rheb* gene encodes a small GTPase, closely related to Ras, that exists either in an active GTP-bound or an inactive GDP-bound state (5). Rheb is inactivated by the tuberous sclerosis complex 1 and 2 (TSC1 and TSC2, respectively) GTPase-activating protein complex that catalyzes the conversion of Rheb-GTP to Rheb-

* This work was supported by Grant-in-aid for Scientific Research CH/11/3/29051 from the Ministry of Education, Culture, Sports, and Science, Japan to Osaka University and Grant RG/11/12/29052 from the British Heart Foundation to King's College London.
[1] To whom correspondence should be addressed: Cardiovascular Division, King's College London, 125 Coldharbour Ln., London SE5 9NU, UK. Tel.: 020-7848-5128; Fax: 020-7848-5193; E-mail: kinya.otsu@kcl.ac.uk.

[2] The abbreviations used are: mTORC1, mammalian target of rapamycin complex 1; TSC, tuberous sclerosis complex; 4E-BP, 4E-binding protein, αMHC-Cre mice, α-myosin heavy chain promoter driven Cre recombinase transgenic mice; LV, left ventricular; PCNA, proliferating cell nuclear antigen; LC3, light chain 3.

GDP (6). The role of Rheb toward mTORC1 activation in the postnatal hearts has not been elucidated.

Protein biosynthesis represents a major cellular process controled by mTORC1, which is coordinately regulated by the mTORC1–4E-BP1 and -4E-BP2 (eukaryotic initiation factor 4E-binding proteins 1 and 2) and mTORC1-p70 S6 kinase axis (3). In mammalian cells, translation is controlled at the initiation step, when the 40 S ribosomal subunit is recruited to the mRNA (7). The capping of the 5′ end of mRNA allows the recruitment of eIF4F, including eIF4E and the 40 S ribosomal subunit to the mRNA 5′-cap structure (8). The phosphorylation of 4E-BP1 by mTORC1 prevents its binding to eIF4E, enabling eIF4E to promote cap-dependent translation (8). The detailed role of the mTORC1-S6 kinase axis in translational control remains to be elucidated (9). S6 kinase phosphorylates several substrates that function in translation and drive protein production.

In addition to the role of mTORC1 in protein synthesis, it plays an important role in protein degradation. There are two protein degradation systems in mammalian cells, namely autophagy and ubiquitin/proteasome systems. mTORC1 suppresses autophagy in mammalian cells (10) by binding and phosphorylating the autophagy-initiating kinase ULK1 (11).

To investigate an *in vivo* role of Rheb, loss-of-function studies have been reported (12, 13). Rheb-deficient embryos died around midgestation with impaired development of the cardiovascular system (12). Rheb-deficient embryonic fibroblasts showed decreased mTORC1 activity, were smaller, and showed impaired proliferation compared with wild-type cells. Embryonic deletion of Rheb1 in neural progenitor cells abolished mTORC1 signaling in developing brain (13).

In adult hearts, Rheb has been reported to be involved in cardiac hypertrophy. Overexpression of Rheb in isolated adult rat cardiomyocytes activated mTORC1 and protein synthesis and induced enlargement of cell surface area (14). Although Rheb was inactivated during acute myocardial ischemia, overexpression of Rheb in the mouse heart reversed the down-regulation of mTORC1 activity during ischemia and increased infarct size accompanied by inhibition of autophagy (15). In the current study, we generated floxed *Rheb* mice to obtain cardiac-specific Rheb-deficient mice to elucidate the role of Rheb in the *in vivo* heart and examine the contribution of Rheb to mTORC1 signaling in postnatal cardiac development. We found that Rheb is not required for mTORC1 signaling during the early postnatal period but becomes essential for mTORC1 signaling and normal cardiac development after transition from proliferation to hypertrophy.

EXPERIMENTAL PROCEDURES

Generation of Cardiac-specific Rheb-deficient Mice—The *Rheb* gene-targeting vector was constructed using a mouse C57BL/6J BAC genomic library (BACPAC Resources Center) as reported previously (16). The targeting vector was electroporated into ES cells (F1; SVJ129 and C57BL/6J), and the transfected ES clones were selected for neomycin resistance according to standard protocols. The neomycin-resistant ES clones with targeted homologous recombination were screened by PCR and further confirmed by Southern blotting. Circular pCAG-FLpe plasmid and pPGK-Puro plasmid was electroporated into the selected ES clones, and the transfected ES clones were selected for puromycin resistance according to the standard protocols. The neomycin cassette excised ES clones were screened by PCR. Southern blotting and karyotyping analyses were performed to obtain ES clones exhibiting the desired homologous recombination and normal karyotype. These targeted ES clones were injected into blastocyst mouse embryos to generate chimeric mice. The chimeric mice were crossed with C57BL/6J mice to validate germ line transmission. The offspring with "floxed" Rheb mice were crossed with transgenic mice expressing *Cre* recombinase under the control of the α-myosin heavy chain promoter (*αMHC-Cre* mice) in the C57BL/6J background (17) to generate cardiac-specific deletion of Rheb. The genotype of the floxed mice was determined by PCR on tail genomic DNA using primers as follows: 5′-GCT GAC ACT CAC TAC AGA ATA ATG-3′ and 5′-CAA TCA TTA ACC TGA CTG GTC TCT-3′ to amplify the wild-type and floxed alleles (296 and ~350 bp, respectively). The primers for the amplification of *αMHC-Cre* are 5′-GAA CAC ACC TGG AAG ATG CTC CT-3′ and 5′- CTG ATT CTG GCA ATT TCG GCA AT-3′ with the amplicon of 427 bp.

To generate double knock-out mice of *Rheb* and *Eif4ebp1*, $Rheb^{flox/+}$;$\alpha MHC\text{-}Cre^{+}$ mice were crossed with $Eif4ebp1^{-/-}$ mice (18) in the C57BL/6J background. To generate double knock-out mice of *Rheb* and *Atg5*, $Rheb^{flox/+}$;$\alpha MHC\text{-}Cre^{+}$ mice were crossed with $Atg5^{flox/flox}$ mice (19) in the C57BL/6J background.

Southern Hybridization—Southern blot analysis of embryonic stem cells was performed as reported previously (17). Genomic DNA was isolated from embryonic stem cells, digested with KpnI, and subjected to Southern blot analysis. The probe used was an 1174-bp PCR fragment amplified with 5′-ACT TCC CTT GTA GTT TAG CGT ATA GCA-3′ and 5′-ACC TAA CTA AAT GAA CAA ACA AAA ATG GCA-3′.

Echocardiographic Assessment—Vevo 770 with a 25-MHz imaging transducer or Vevo 2100 with a 40-MHz imaging transducer (Visual Sonics) was used for noninvasive transthoracic echocardiographic analysis on awake mice in water at 37 °C. Two-dimensional guided M-mode tracings were recorded. The internal diameter of the left ventricle in the short axis plane was measured at end diastole and end systole from M-mode recordings just below the tips of the mitral valve leaflets. The interventricular and left ventricular (LV) posterior wall thicknesses were measured at the end diastole.

Histological Analysis—Hematoxylin/eosin or Azan-Mallory staining was performed on paraffin-embedded sections. The cross-sectional areas of cardiomyocytes were determined as described previously (20). To determine the number of cells undergoing apoptosis, we performed a TUNEL assay on paraffin-embedded heart sections, using an *in situ* apoptosis detection kit (Takara Bio, Inc.). For electron microscopy, the hearts were perfused in retrograde and fixed with 2.5% glutaraldehyde (Wako) in 0.1 M phosphate buffer (pH 7.4). The LV tissues were processed for transmission electron microscopy H-7650 (Hitachi) as described previously (21). To evaluate the sarcomeric to cytosolic area ratio, the area of sarcomere or cytosol in the micrograph taken at 1000-fold magnification was evaluated

using NIH ImageJ software (version 1.43u) for 20 fields per mouse.

Western Blot Analysis—Protein homogenates were subjected to Western blot analysis using antibodies against Rheb, eIF4E-BP1, proliferating cell nuclear antigen (PCNA; Abcam), cleaved caspase 3, phospho-eIF4E-BP1 (Ser-65), phospho-eIF4E-BP1 (Thr-70), phospho-eIF4E-BP1 (Thr-37/Thr-46), S6 ribosomal protein, phospho-S6 ribosomal protein, AKT, phospho-AKT (Thr-308), phospho-AKT (Ser-473), LC-3, PRAS40, phospho-PRAS40 and α-tubulin (Cell Signaling Technology), ubiquitin (Dako Cytomation), p62 (PROGEN Biotechnik) and GAPDH (Santa Cruz Biotechnology). NIH ImageJ software (version 1.43u) was used to perform densitometric analyses.

Quantitative Real-time RT-PCR—We isolated total RNA from the ventricle for analysis using the TRIzol reagent (Invitrogen). We determined mRNA levels for *Nppa*, *Nppb*, collagen type 1 α2 (*Col1a2*), and GAPDH by quantitative RT-PCR. For reverse transcription and amplification, we used the TaqMan Reverse Transcription Reagents (Applied Biosystems) and Platinum Quantitative PCR SuperMix-UDG (Invitrogen). The PCR primers and probes of *Nppa* (assay ID Mm01255747_g1), *Nppb* (assay ID Mm00435304_g1), *Col1a2* (assay ID Mm01165187_m1), and GAPDH (4352339E) were obtained from Applied Biosystems. We constructed RT-PCR standard curves using the corresponding cDNA. All data were normalized to GAPDH content and are expressed as fold increase over the control group.

Myocyte Isolation and Cell Surface Area—Myocytes were enzymatically isolated from neonatal hearts. The cannulated heart was attached to Langendorff apparatus for coronary perfusion with calcium-free solution (120 mM NaCl, 5.5 mM KCl, 1.2 mM NaH_2PO_4, 20 mM $NaHCO_3$, 1.6 mM $MgCl_2$, 5.6 mM glucose, 5 mM taurine). After 2 min, the perfusion solution was switched to the calcium-free solution containing 350 units/ml collagenase (Worthington) and perfused for an additional 15 min. The heart was then minced in the calcium-free solution containing 1 mg/ml BSA (Sigma), and isolated cardiomyocytes were obtained. Cell images were taken under a phase contrast microscope DP21 (Olympus). NIH ImageJ software (version 1.43u) was used to analyze cell surface area. One hundred myocytes from each heart were used for the measurement of cell surface area.

Polysome Analysis—Polysome profile analysis was carried out as described previously (22). Hearts were lysed in a hypotonic lysis buffer (5 mM Tris-HCl (pH 7.5), 2.5 mM $MgCl_2$, 1.5 mM KCl, 100 mg/ml cycloheximide, 2 mM DTT, 0.5% Triton X-100, and 0.5% sodium deoxycholate). Lysates were loaded onto 10–50% sucrose density gradients (20 mM HEPES-KOH (pH 7.6), 100 mM KCl, 5 mM $MgCl_2$) and centrifuged at 40,000 rpm for 2.5 h at 4 °C using an ultracentrifuge Optima L-90K and SW 41 Ti (Beckman). Gradients were fractionated, and absorbance at 254 nm was continuously recorded using a gradient fractionator (BioComp Instruments) and a spectrophotometer UV-3100PC (Shimazu).

Immunoprecipitation—The hearts from 8-day-old mice were homogenized in TEN buffer (100 mM Tris-HCl, (pH 7.5), 100 mM NaCl, 10 mM EDTA, 0.5% Nonidet P-40) supplemented with 1× phosphatase inhibitor mixture (Roche Applied Science) and 1× Complete protease inhibitor mixture (Roche Applied Science) and clarified by centrifugation at 15,000 rpm for 20 min at 4 °C. Detergent-soluble fractions were incubated with protein A-Sepharose (GE Healthcare) preincubated with rabbit monoclonal anti-4E-BP1 antibody (Cell Signaling Technology), followed by overnight rotation at 4 °C. Protein A-Sepharose complexes were sequentially washed twice with TEN buffer supplemented with 500 mM NaCl and twice with TEN buffer alone. Immunoprecipitates were eluted by heating at 95 °C for 5 min in 2× Laemmli sample buffer containing 2% 2-mercaptoethanol. Immunoprecipitates and input lysates were resolved by SDS-PAGE and subjected to Western blot analysis using antibodies 4E-BP1 and eIF4E (Abcam).

Statistics—Results are expressed as the mean ± S.E. Comparisons between two groups were performed using Student's *t* test. One-way analysis of variance with Bonferroni post hoc test was used for multiple comparisons. The Kaplan-Meier method with a log-rank test was used for survival analysis. $p < 0.05$ was considered statistically significant.

Study Approval—Experiments using animals in this study were carried out under the supervision of the Animal Research Committee of Osaka University and in accordance with the Guidelines for Animal Experiments of Osaka University and the Japanese Act on Welfare and Management of Animals (no. 105).

RESULTS

Generation of Cardiac-specific Rheb-deficient Mice—To investigate the role of Rheb in the heart, we generated cardiac-specific Rheb-deficient mice. To obtain cardiac-specific Rheb-deficient mice, conditional inactivation of the *Rheb* gene was achieved by the inserting *loxP* sites cloned 5′ and 3′ of exon 3 (Fig. 1*A*). Selection cassettes comprising a neomycin resistance gene (*neo*), flanking two flippase recognition target sites, for positive selection and a diphtheria toxin gene for negative selection were positioned between exon 3 and the downstream *loxP* site and at the 3′ end of the targeting vector, respectively (Fig. 1*A*). Homologous recombinants were identified by PCR and Southern blotting. The ES cells with the *Rheb*-floxed allele and the selection marker gene, that is, the *PGK-neo* cassette, were transfected with plasmid encoding *FLpe* recombinase to obtain *Rheb*-floxed ES cells without the *PGK-neo* cassette, which were identified by PCR and Southern blotting (Fig. 1*B*). The homozygous *Rheb*-floxed mice ($Rheb^{flox/flox}$) appeared normal and were externally indistinguishable from littermates of other genotypes. To investigate the *in vivo* role of Rheb, we generated cardiac-specific Rheb-deficient mice. We crossed $Rheb^{flox/flox}$ mice with α-myosin heavy chain promoter-driven *Cre* recombinase transgenic mice (17) (*αMHC-Cre*) to generate $Rheb^{flox/flox}$;$\alpha MHC\text{-}Cre^{+}$ mice ($Rheb^{-/-}$). We used $Rheb^{flox/flox}$;$\alpha MHC\text{-}Cre^{-}$ littermates as controls ($Rheb^{+/+}$). Immunoblot analysis of heart extracts from mice indicated that there were no significant differences in Rheb protein level in $Rheb^{+/+}$ hearts among at postnatal day 3, 5, and 8 (Fig. 1*C*). We observed a 70% reduction in Rheb protein level in $Rheb^{-/-}$ hearts relative to $Rheb^{+/+}$ hearts at postnatal day 3 (Fig. 1*D*). It has been reported that the αMHC promoter becomes active in cardiomyocytes between embryonic days 7.5

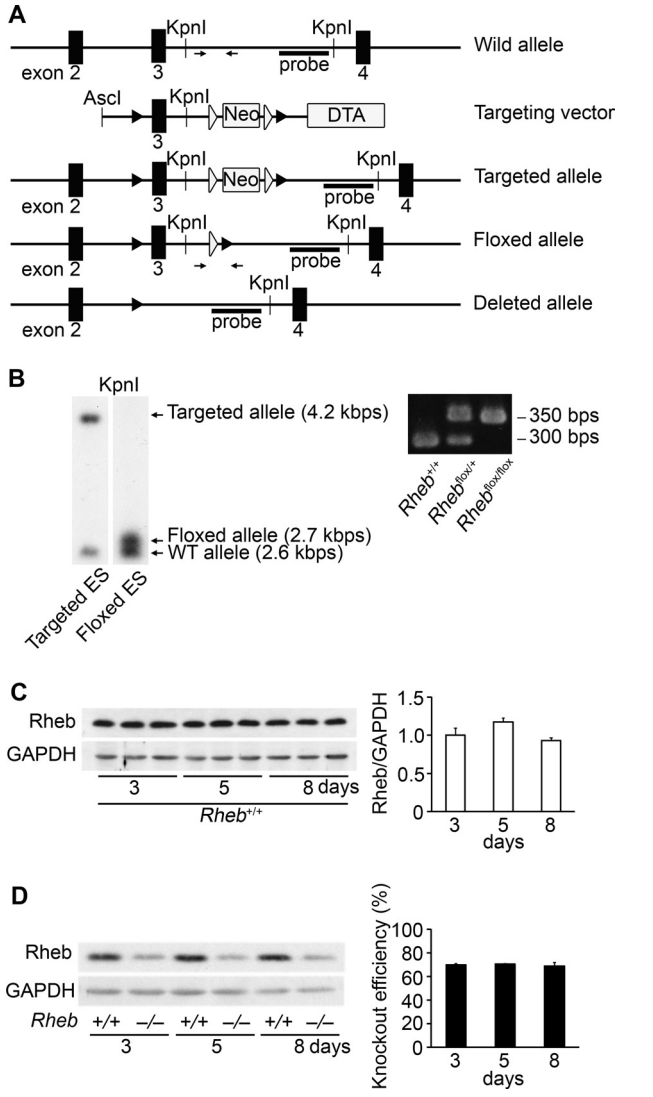

FIGURE 1. **Targeted modification of the *Rheb* gene.** *A*, schematic structures of genomic *Rheb* sequences, the targeting construct, the targeted allele, the floxed allele, and the $Rheb^{-/-}$ allele (from *top* to *bottom*). The *black* and *white arrowheads* represent *loxP* and flippase recognition target sites, respectively. The targeting construct includes the *PGK-neo* cassette flanked by flippase recognition target sites and a diphtheria toxin gene (*DTA*). The *arrows* correspond to the primer sequences for PCR screening. The *bar* labeled *probe* corresponds to the sequence used for Southern blotting analysis in *B*. *B*, genomic analysis of *ES cells* (*left panel*). Genomic DNA was isolated from ES cells, digested with KpnI, and analyzed by Southern blotting with the probe. Shown is genomic analysis of mouse tails (*right panel*). Genomic DNA was isolated from mouse tail and subjected to PCR analysis. *C* and *D*, protein expression of Rheb at postnatal days 3, 5, and 8. Heart extracts from $Rheb^{+/+}$ (*C* and *D*) and $Rheb^{-/-}$ (*D*) at postnatal day 3, 5, or 8 were subjected to Western blot analysis. The average value at postnatal day 3 was set equal to 1 (*C*). *Right panels* show densitometric analysis ($n = 3$). Values are expressed as the mean ± S.E. *, $p < 0.05$.

and 8 in mice (23). In fact, there were no significant differences in relative Rheb protein level to $Rheb^{+/+}$ in $Rheb^{-/-}$ hearts at postnatal days 3, 5, and 8 (70, 70.5, and 68.9% reduction at postnatal day 3, 5, and 8, respectively) (Fig. 1*D*). Expected Mendelian ratios of $Rheb^{flox/flox}$;*αMHC-Cre*$^{+}$, $Rheb^{flox/flox}$;*αMHC-Cre*$^{-}$, $Rheb^{flox/+}$;*αMHC-Cre*$^{+}$, $Rheb^{flox/+}$;*αMHC-Cre*$^{-}$ mice ($n = 115$, 140, 114, and 118, respectively) were detected at postnatal day 3 among the offspring of $Rheb^{flox/flox}$;*αMHC-Cre*$^{-}$ and $Rheb^{flox/+}$;*αMHC-Cre*$^{+}$ mice, indicating no significant embryonic lethality.

Cardiac-specific Deletion of Rheb Resulted in Premature Death and Cardiac Dysfunction after Early Postnatal Period—$Rheb^{-/-}$ mice started to die at postnatal day 8 (Fig. 2*A*). At postnatal day 10, all $Rheb^{-/-}$ mice had died, whereas no $Rheb^{+/+}$ mice died at that time. Physiological parameters such as body weight, heart weight and lung weight were not significantly different between $Rheb^{-/-}$ and $Rheb^{+/+}$ mice at postnatal days 3 and 5 (Fig. 2*B*). Body weight increased with age both in $Rheb^{-/-}$ and $Rheb^{+/+}$ mice. The heart weight at postnatal day 8 was greater than that at postnatal day 3 or 5 in $Rheb^{+/+}$ mice. In $Rheb^{-/-}$ mice, the heart weight at postnatal day 8 was greater than that at postnatal day 3 but was not significantly different from that at day 5. The heart weight in $Rheb^{-/-}$ mice was significantly lower than that in $Rheb^{+/+}$ mice at postnatal day 8. The ratio of heart-to-body weight in $Rheb^{-/-}$ mice at postnatal day 8 was significantly lower than that in $Rheb^{-/-}$ at postnatal day 3 or 5 or that in $Rheb^{+/+}$ mice at postnatal day 8. We performed echocardiographic analysis on $Rheb^{-/-}$ mice. The echocardiographic parameters were not significantly different at postnatal day 5 between $Rheb^{-/-}$ and $Rheb^{+/+}$ mice (Fig. 2*D*). However, the diastolic interventricular septum thickness and diastolic LV posterior wall thickness in $Rheb^{-/-}$ mice were significantly smaller than those in $Rheb^{+/+}$ mice at postnatal day 8. The end-diastolic and systolic LV dimensions were significantly larger and LV fractional shortening was significantly reduced in $Rheb^{-/-}$ mice at postnatal day 8 compared with $Rheb^{+/+}$ mice at postnatal day 8 or $Rheb^{-/-}$ mice at postnatal day 5. We evaluated the level of atrial natriuretic factor and brain natriuretic peptide mRNA expression, which are biochemical markers for adverse cardiac remodeling, by means of quantitative RT-PCR at postnatal day 8 (Fig. 3*A*). The mRNA levels of atrial natriuretic factor and brain natriuretic peptide were significantly elevated in $Rheb^{-/-}$ mice compared with $Rheb^{+/+}$ mice. The $Rheb^{-/-}$ hearts appeared to exhibit lower Hematoxylin/eosin stainability at postnatal day 8 (Fig. 3*B*). The mRNA level for collagen α-2(I) chain increased in $Rheb^{-/-}$ hearts (Fig. 3*A*), whereas Azan-Mallory staining indicated a slight increase in the extent of fibrosis at postnatal day 8 (Fig. 3*C*). These data indicate that $Rheb^{-/-}$ mice exhibited normal cardiac function until postnatal day 5 but developed cardiac dysfunction at postnatal day 8. Thus, Rheb is not required for embryonic heart development and maintenance of cardiac structure and function until postnatal day 5.

TUNEL assay revealed that there was no significant difference in the number of TUNEL-positive cardiomyocytes between $Rheb^{-/-}$ and $Rheb^{+/+}$ hearts at postnatal day 8 (Fig. 3*D*). Furthermore, there was no significant difference in the level of cleaved caspase 3 (Fig. 3*E*). These results suggest that apoptosis was not a major cause for the development of dilated cardiomyopathy in $Rheb^{-/-}$ mice.

Histological Analysis of Rheb-deficient Mice Revealed Small Cardiomyocyte Size—Because we observed a lower ratio of heart weight/body weight in $Rheb^{-/-}$ mice at postnatal day 8, we estimated cross-sectional area of cardiomyocytes on heart sections at postnatal day 3, 5, and 8 (Fig. 4, *A* and *B*). There were no significant differences in cross-sectional area of cardiomyocytes between 3 and 5 days after birth either in $Rheb^{-/-}$ or $Rheb^{+/+}$ mice or between $Rheb^{-/-}$ and $Rheb^{+/+}$ mice at post-

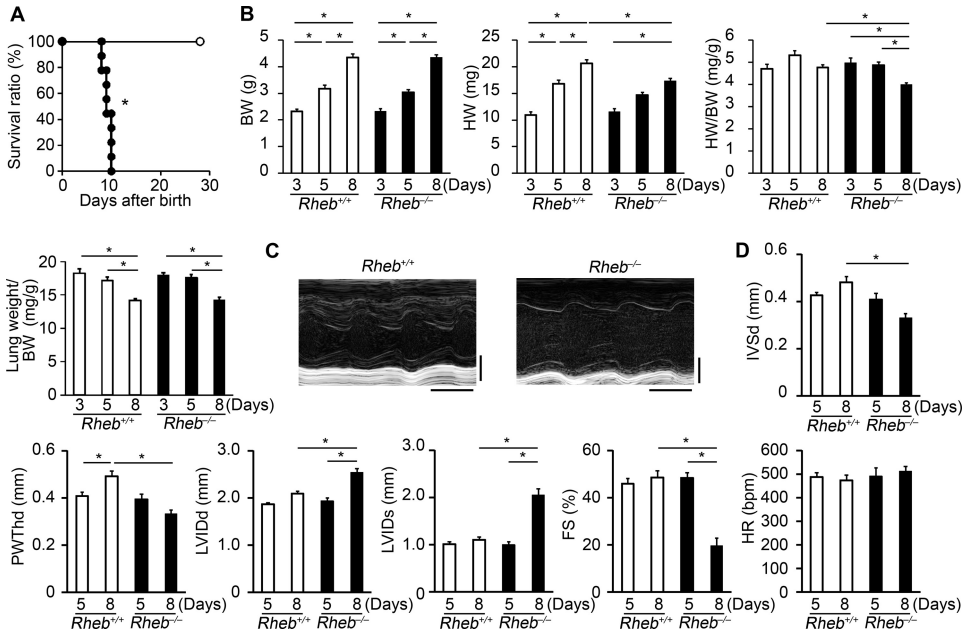

FIGURE 2. **Physiological and echocardiographic characterization of *Rheb*$^{-/-}$ mice.** *A*, survival ratio of *Rheb*$^{-/-}$ and *Rheb*$^{+/+}$ mice after birth. *Open* and *closed circles* represent *Rheb*$^{+/+}$ ($n = 11$) and *Rheb*$^{-/-}$ mice ($n = 9$), respectively. *, $p < 0.05$. *B*, physiological parameters of *Rheb*$^{-/-}$ and *Rheb*$^{+/+}$ mice at postnatal days 3 ($n = 8$ per group), 5 ($n = 10$–11 per group), and 8 ($n = 16$–20 per group). *Open* and *closed bars* represent *Rheb*$^{+/+}$ and *Rheb*$^{-/-}$ mice, respectively. Values are expressed as the mean ± S.E. *, $p < 0.05$. *BW* and *HW* indicate body weight and heart weight, respectively. *C*, representative M-mode echocardiographic tracings at postnatal day 8. *Scale bars*, 0.1 s and 1 mm, respectively. *D*, echocardiographic parameters of *Rheb*$^{-/-}$ and *Rheb*$^{+/+}$ mice at postnatal days 5 ($n = 6$–7 per group) and 8 ($n = 8$–9 per group). *IVSd* indicates diastolic interventricular septum thickness; *PWThd*, diastolic left ventricular posterior wall thickness; *LVIDd*, end diastolic left ventricle internal dimension; *LVIDs*, end-systolic left ventricle internal dimension; *FS*, left ventricle fractional shortening; *HR*, heart rate. *Open* and *closed bars* represent *Rheb*$^{+/+}$ and *Rheb*$^{-/-}$ mice, respectively. Values are expressed as the mean ± S.E. *, $p < 0.05$.

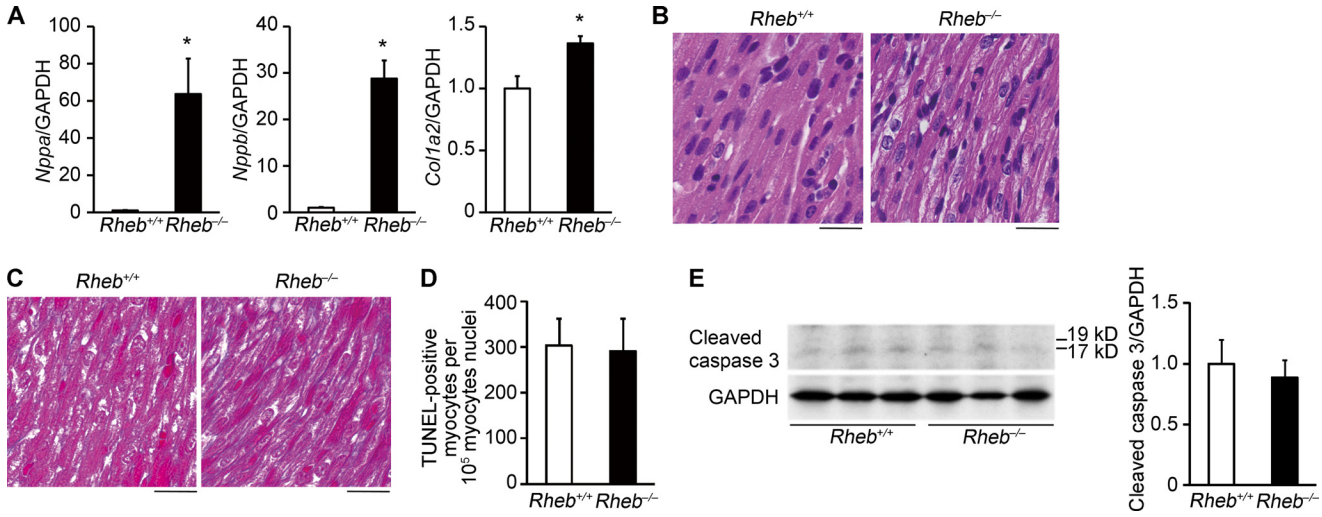

FIGURE 3. **Biochemical and histological characterization of *Rheb*$^{-/-}$ mice at postnatal day 8.** *A*, mRNA expressions of *Nppa*, *Nppb*, and *Col1a2* ($n = 3$–5). GAPDH was used as the loading control. *Open* and *closed bars* represent *Rheb*$^{+/+}$ and *Rheb*$^{-/-}$ mice, respectively. The average value for *Rheb*$^{+/+}$ mice was set equal to 1. Values are expressed as the mean ± S.E. *, $p < 0.05$ *versus* *Rheb*$^{+/+}$ controls. *B*, hematoxylin/eosin-stained heart sections. *Scale bar*, 20 μm. *C*, Azan-Mallory-stained heart sections. *Scale bar*, 20 μm. *D*. number of TUNEL-positive cardiomyocytes. Values are expressed as the mean ± S.E. ($n = 3$). *E*, Western blot analysis of heart extracts using cleaved caspase 3 antibody at postnatal day 8. *Right panel* shows densitometric analysis ($n = 3$). The average value for *Rheb*$^{+/+}$ mice was set equal to 1. Values are expressed as the mean ± S.E.

natal day 3 or 5. In *Rheb*$^{+/+}$ hearts, the cross-sectional area at postnatal day 8 was larger than that at postnatal day 5. However, there was no significant difference in the cross-sectional area between 5 and 8 days after birth in *Rheb*$^{-/-}$ mice. As a result, *Rheb*$^{-/-}$ hearts exhibited smaller cross-sectional area than *Rheb*$^{+/+}$ hearts at postnatal day 8. To confirm this result, we isolated cardiomyocytes from the mice and estimated the cell surface area (Fig. 4, *C* and *D*). In *Rheb*$^{+/+}$ mice, the cell surface area increased with age. Although the cell surface area increased by 35.5% between 3 and 5 days after birth, it increased by 88.9% for the next 3 days. In *Rheb*$^{-/-}$ mice, the cell surface area increased by 36.6% between 3 and 5 days after birth, but there was no further increase in the cell surface area between 5 and 8 days after birth. Consequently, *Rheb*$^{-/-}$ cardiomyocytes exhibited smaller cell surface area than *Rheb*$^{+/+}$ cardiomyocytes at postnatal day 8. We examined the protein level of PCNA to evaluate the level of proliferation (Fig. 5). In *Rheb*$^{+/+}$ hearts, the level of PCNA at postnatal day 8 was lower than that

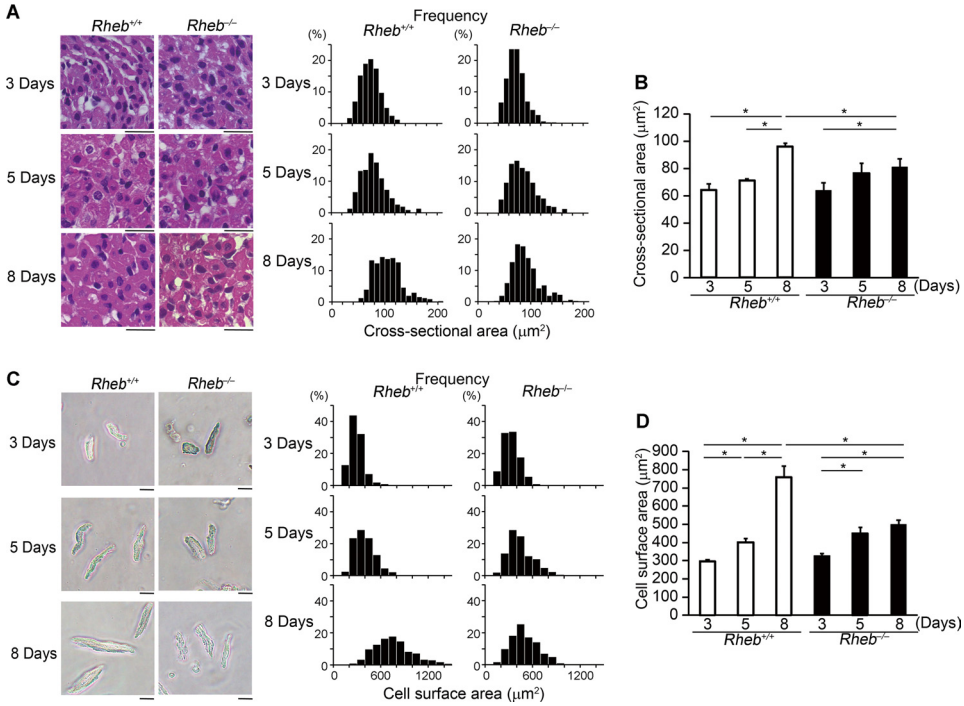

FIGURE 4. **Cardiomyocyte size of *Rheb*$^{-/-}$ mice.** *A*, hematoxylin/eosin-stained heart sections at postnatal day 3, 5, and 8. *Scale bar*, 20 μm. *Right panels* show histograms of cross-sectional area of cardiomyocytes. *B*, cross-sectional area of cardiomyocytes. Values are expressed as the mean ± S.E. ($n = 3–4$ per group). *, $p < 0.05$. *C*, isolated cardiomyocytes from *Rheb*$^{-/-}$ mice. *Scale bar*, 20 μm. *Right panels* show histograms of cell surface area of cardiomyocytes. *D*, cell surface area of isolated cardiomyocytes. Values are expressed as the mean ± S.E. ($n = 3–4$ per group). *, $p < 0.05$.

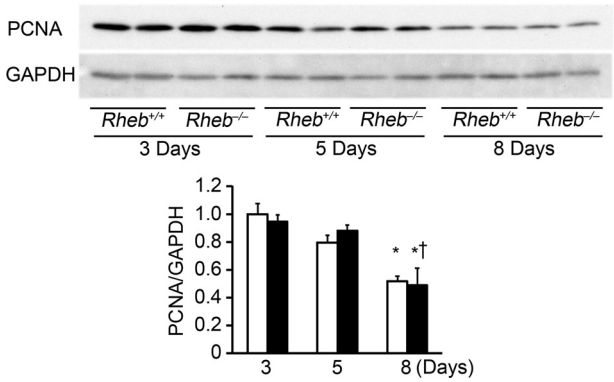

FIGURE 5. **Proliferation in *Rheb*$^{-/-}$ hearts.** Western blot analysis of heart extracts using anti-PCNA. Heart extracts from *Rheb*$^{-/-}$ and *Rheb*$^{+/+}$ mice at postnatal days 3, 5, and 8. *Lower panel* shows densitometric analysis ($n = 3$). *Open* and *closed bars* represent *Rheb*$^{+/+}$ and *Rheb*$^{-/-}$ mice, respectively. The average value for *Rheb*$^{+/+}$ mice at postnatal day 3 was set equal to 1. Values are expressed as the mean ± S.E. *, $p < 0.05$ *versus* corresponding mice at postnatal day 3. †, $p < 0.05$ *versus* corresponding mice at postnatal day 5.

at postnatal day 3. There was no significant difference in the PCNA protein level between *Rheb*$^{-/-}$ and *Rheb*$^{+/+}$ mice at postnatal day 3, 5, or 8. These results suggest that Rheb is not related to cardiomyocyte proliferation but is essential for postnatal hypertrophic growth of cardiomyocytes.

mTORC1 Signaling Was Impaired by Deletion of Rheb after Early Postnatal Period—The extent of reduction in Rheb protein level in *Rheb*$^{-/-}$ hearts compared with *Rheb*$^{+/+}$ hearts was similar at postnatal days 3, 5, and 8 (Fig. 1*D*). Nevertheless, there was no significant difference in the phosphorylation level of S6 or 4E-BP1 between *Rheb*$^{-/-}$ and *Rheb*$^{+/+}$ mice at postnatal day 3, indicating preservation of mTORC1 signaling (Fig. 6, *A–D*). The phosphorylation level of S6 or 4E-BP1 was significantly attenuated in *Rheb*$^{-/-}$ hearts compared with the control at postnatal day 5 or 8. The phosphorylation of 4E-BP1 was further analyzed using its phosphorylation site-specific antibodies. The phosphorylation levels of Thr-37/Thr-46 and Ser-65 in 4E-BP1 were attenuated in *Rheb*$^{-/-}$ hearts at postnatal day 8. It has been reported that deletion of Rheb resulted in an increase in Akt phosphorylation, suggesting a negative feedback in the mTORC1 signaling pathway (12). Consistent with the existence of a negative feedback loop, the phosphorylation level of Akt in *Rheb*$^{-/-}$ hearts was increased at postnatal day 5 or 8, but not at day 3, compared with *Rheb*$^{+/+}$ hearts. The interaction of 4E-BP1 with eIF4E was enhanced in *Rheb*$^{-/-}$ hearts (Fig. 6*E*). The phosphorylation level of PRAS40 was increased in *Rheb*$^{-/-}$ hearts at postnatal day 3 (Fig. 6*F*).

Rapamycin, an inhibitor of mTORC1, attenuated the PCNA protein level, the phosphorylation level of S6 or 4E-BP1, body weight, heart weight, and the ratio of heart-to-body weight in *Rheb*$^{-/-}$ and *Rheb*$^{+/+}$ mice at postnatal day 3 (Fig. 7, *A* and *B*). There was no significant difference in body weight, heart weight, or the ratio of heart-to-body weight between rapamycin-treated *Rheb*$^{-/-}$ and *Rheb*$^{+/+}$ mice at postnatal day 3. At postnatal day 8, rapamycin attenuated the PCNA protein level and the phosphorylation level of S6 or 4E-BP1 in *Rheb*$^{-/-}$ and *Rheb*$^{+/+}$ mice. Heart weight or the ratio of heart-to-body weight in *Rheb*$^{+/+}$ mice was greater than that in *Rheb*$^{-/-}$ mice. Rapamycin decreased the ratio of heart-to-body weight in *Rheb*$^{+/+}$ but not in *Rheb*$^{-/-}$ mice.

Sarcomere Maturation and mRNA Translation Were Attenuated in Rheb$^{-/-}$ *Hearts*—To identify a molecular mechanism underlying the cardiac phenotypes observed in *Rheb*$^{-/-}$ mice, we performed ultrastructural analysis on the hearts (Fig. 8, *A*

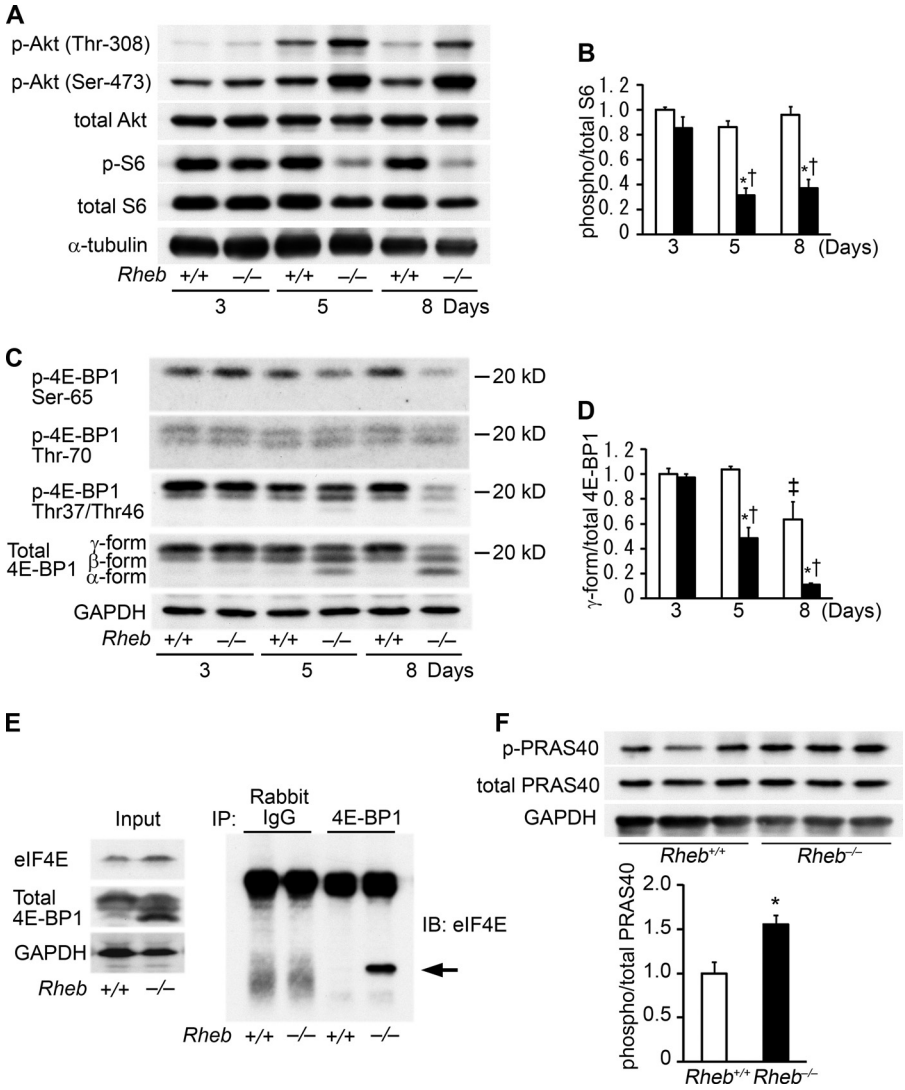

FIGURE 6. **Signal transduction in *Rheb*$^{-/-}$ hearts.** *Open* and *closed bars* represent *Rheb*$^{+/+}$ and *Rheb*$^{-/-}$ mice, respectively. *A*, heart extracts from 3-, 5-, and 8-day-old mice were immunoblotted with the indicated antibodies. *B*, average of phospho-S6 to total S6 ratios from heart extracts ($n = 3$). The average value for *Rheb*$^{+/+}$ mice at postnatal day 3 was set equal to 1. *, $p < 0.05$ *versus* corresponding *Rheb*$^{+/+}$ controls. †, $p < 0.05$ *versus* corresponding mice at postnatal day 3. *C*, Western blot analysis on 4E-BP1. Heart extracts were immunoblotted (*IB*) with the indicated antibodies. *D*, average of γ-form 4E-BP1 to total 4E-BP1 ratios from heart extracts ($n = 3$). The average value for *Rheb*$^{+/+}$ mice at postnatal day 3 was set equal to 1. *, $p < 0.05$ *versus* corresponding *Rheb*$^{+/+}$ controls. †, $p < 0.05$ *versus* corresponding mice at postnatal day 3. ‡, $p < 0.05$ *versus* corresponding mice at postnatal day 5. *E*, coimmunoprecipitation of 4E-BP1 and eIF4E in *Rheb*$^{+/+}$ and *Rheb*$^{-/-}$ heart lysates at postnatal day 8 followed by Western blot analysis. *F*, Rheb-independent pathway at postnatal day 3. Western blot analysis of heart extracts using anti-phospho-PRAS40 or PRAS40 antibody. Heart extracts from *Rheb*$^{-/-}$ and *Rheb*$^{+/+}$ mice at postnatal day 3. The *lower panel* shows densitometric analysis ($n = 3$). The average value for *Rheb*$^{+/+}$ mice was set equal to 1. Values are expressed as the mean ± S.E. *, $p < 0.05$.

and *B*). At postnatal day 3 or 5, the sarcomere structures in both *Rheb*$^{-/-}$ and *Rheb*$^{+/+}$ were immature, indicated by a narrow sarcomere width. There was no significant difference in sarcomeric to cytosolic area ratio between *Rheb*$^{-/-}$ and *Rheb*$^{+/+}$ mice at postnatal day 3 or 5. At postnatal day 8, the width of the sarcomere became greater in *Rheb*$^{+/+}$ mice, but it remained narrow in *Rheb*$^{-/-}$ mice. The sarcomeric to cytosolic area ratio was increased by 35% in *Rheb*$^{+/+}$ hearts between 5 and 8 days after birth, whereas there was no significant difference during this period in *Rheb*$^{-/-}$ mice. The ratio was larger in *Rheb*$^{+/+}$ hearts than that in *Rheb*$^{-/-}$ hearts at postnatal day 8. These results indicate that sarcomere maturation was impaired in *Rheb*$^{-/-}$ hearts. There was no significant difference in the number of mitochondria per cell area between 5 and 8 days after birth in *Rheb*$^{-/-}$ or *Rheb*$^{+/+}$ mice (Fig. 8*C*).

It has been reported that mTORC1 promotes cell proliferation through enhanced translation of mRNAs mediated through 4E-BP1 (24). We thus examined the translation activity by estimating the association of ribosomes with mRNA at various time points after birth (Fig. 8*D*). In this assay, the number of ribosomes within the polysomal fraction of mRNA is a reflection of *de novo* protein synthesis (25). *Rheb* ablation caused a decrease in polysomal fractions from postnatal day 5, indicating a reduction in translation in *Rheb*$^{-/-}$ hearts.

Autophagy Was Not Involved in the Development of Cardiomyopathy in Rheb$^{-/-}$ *Hearts*—Determinants for cell size should be the levels of protein synthesis and degradation. There are two protein degradation systems in mammalian cells, namely the autophagy and ubiquitin/proteasome systems. We have previously reported that constitutive autophagy is critical

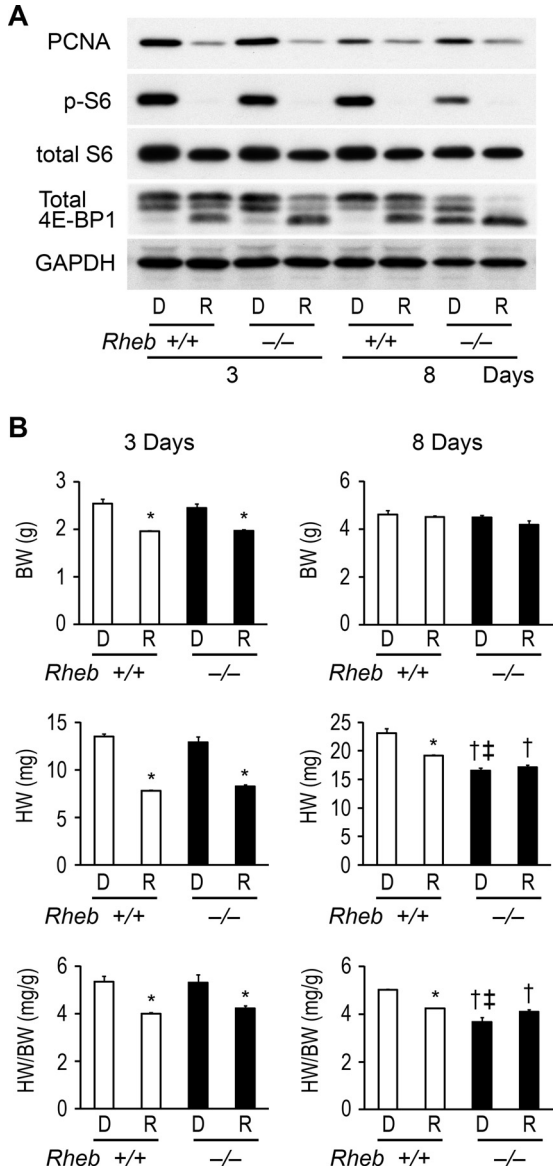

FIGURE 7. **Effect of rapamycin on the proliferation and the cardiac growth.** Rapamycin (2.5 mg/kg) or dimethyl sulfoxide was administered intraperitoneally at postnatal day 1 and 2 and analyzed at postnatal day 3. When mice were analyzed at postnatal day 8, rapamycin was administered at postnatal day 7. *D* and *R* indicate dimethyl sulfoxide and rapamycin-treated groups, respectively. *A*, heart extracts were immunoblotted with the indicated antibodies. *B*. physiological parameters. *BW* and *HW* indicate body weight and heart weight, respectively. Values are expressed as the mean ± S.E. ($n = 3$ per group). *, $p < 0.05$ *versus* corresponding dimethyl sulfoxide-treated mice. †, $p < 0.05$ *versus* dimethyl sulfoxide-treated *Rheb*$^{+/+}$ control mice. ‡, $p < 0.05$ *versus* rapamycin-treated *Rheb*$^{+/+}$ control mice.

for the maintenance of cardiac function, whereas inducible autophagy plays an important role to protect hearts from hemodynamic stress (21). mTORC1 is known to be an important negative regulator of autophagy in mammalian cells (10). We investigated the autophagic activity in *Rheb*$^{-/-}$ hearts by immunoblot for microtubule-associated protein light chain 3 (LC3) and p62 at postnatal day 8 (Fig. 9*A*). Conversion of LC3-I to LC3-II is an essential step for autophagosome formation. There was no significant difference in the ratio of LC3-II to α-tubulin between in *Rheb*$^{-/-}$ and *Rheb*$^{+/+}$ hearts, whereas the ratio of LC3-II to LC3-I increased in *Rheb*$^{-/-}$ hearts. There was no significant difference in the level of p62, a marker for autophagy flux, between *Rheb*$^{-/-}$ and *Rheb*$^{+/+}$ hearts. These suggest that autophagy flux was not enhanced in *Rheb*$^{-/-}$ hearts compared with *Rheb*$^{+/+}$ hearts. We detected no significant difference in levels of ubiquitinated proteins between *Rheb*$^{-/-}$ and *Rheb*$^{+/+}$ hearts (Fig. 9*B*).

To exclude the contribution of autophagy to cardiomyopathic phenotypes observed in *Rheb*$^{-/-}$ mice, we generated cardiac-specific double knock-out mice of *Rheb* and *Atg5*, which is an essential molecule for autophagy. Ablation of *Atg5* resulted in a decrease in the protein level of LC3-II in *Rheb*$^{-/-}$ hearts (Fig. 9*C*). However, ablation of *Atg5* had no effect on the survival of *Rheb*$^{-/-}$ mice, suggesting that autophagy was not related to the premature death of *Rheb*$^{-/-}$ mice (Fig. 9*C*).

Ablation of Eif4ebp1 Improved Survival, Cardiac Function, and Hypertrophic Growth in Rheb$^{-/-}$ *Mice*—Because it has been reported that deletion of S6 kinases did not attenuate pathological, physiological, or insulin-like growth factor 1 receptor-phosphoinositide 3-kinase-induced cardiac hypertrophy (26), we examined the contribution of the decrease in 4E-BP1 phosphorylation to the observed phenotypes in *Rheb*$^{-/-}$ mice by generating *Rheb*$^{-/-}$;*Eif4ebp1*$^{-/-}$ mice. Ablation of *Eif4ebp1* resulted in a significant improvement of survival in *Rheb*$^{-/-}$ mice (Fig. 10*A*). Echocardiographic analysis on mice at postnatal day 8 showed larger diastolic interventricular septum thickness and posterior wall thickness, smaller end diastolic and systolic LV dimensions, and higher fractional shortening in *Rheb*$^{-/-}$;*Eif4ebp1*$^{-/-}$ mice than those in *Rheb*$^{-/-}$;*Eif4ebp1*$^{+/+}$ mice (Fig. 10, *B* and *C*). Furthermore, ablation of *Eif4ebp1* led to increases in heart weight, the ratio of heart weight to body weight, hematoxylin/eosin stainability, and cross-sectional area (Fig. 10, *D–F*). *Rheb*$^{-/-}$;*Eif4ebp1*$^{-/-}$ mice showed wider and more mature sarcomeres compared with control *Rheb*$^{-/-}$;*Eif4ebp1*$^{+/+}$ mice at postnatal day 8 (Fig. 10*G*). *Eif4ebp1* ablation caused an increase in polysomal fraction at postnatal day 8 in *Rheb*$^{-/-}$ hearts (Fig. 10*H*).

DISCUSSION

In this study, we analyzed the *in vivo* function of Rheb, a vital regulator of mTORC1 signaling, in the heart by conditionally deleting Rheb from cardiomyocytes. We showed that Rheb is not essential for embryonic and early postnatal heart development but essential for heart development beyond postnatal day 5. Conventional Rheb-deficient mice died around midgestation due to impaired development of the cardiovascular system (12). Our results indicate that this impaired development of the cardiovascular system could be the secondary consequences of Rheb deletion. Rheb-dependent mTORC1 activation is indispensable for cardiac hypertrophic growth from postnatal day 5. However, we observed the activation of S6 kinase and 4E-BP1 at postnatal day 3 in *Rheb*$^{-/-}$ mice. Thus, Rheb is not essential for the mTORC1 activation during neonatal cardiac development soon after birth. Possibly, an isofom of Rheb such as RhebL1 (27) partially compensates for the loss of Rheb. Alternatively, mTORC1 may exhibit Rheb-independent activity in *in vivo* hearts. Our experiments using rapamycin indicate that Rheb-independent mTORC1 pathway exists at postnatal days 3 and 8

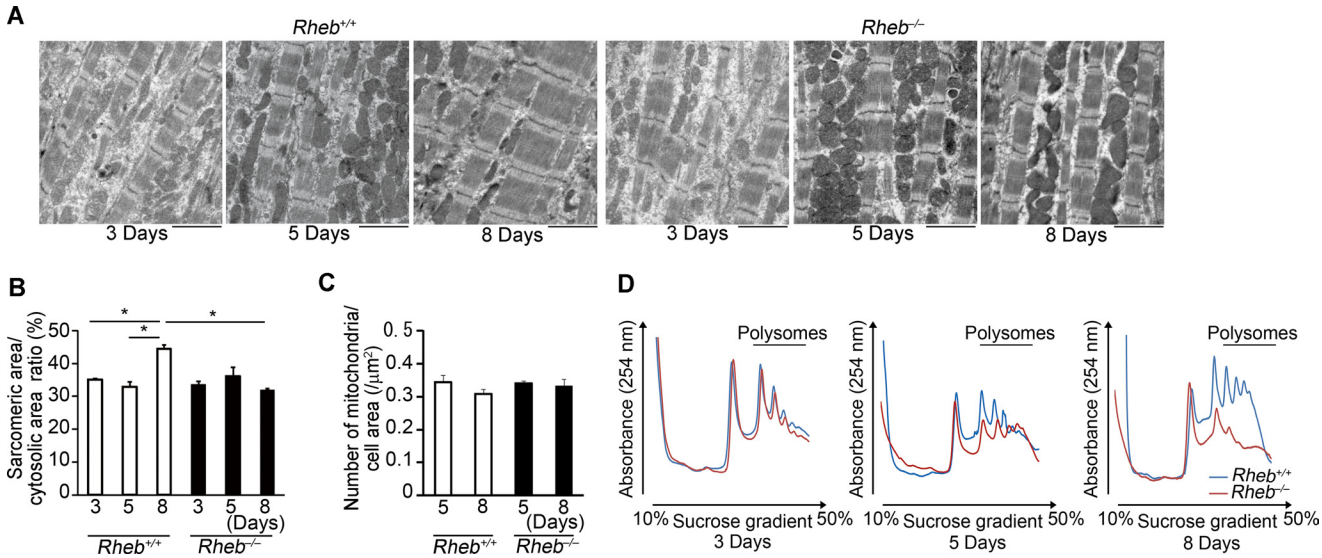

FIGURE 8. **Sarcomeric maturation and protein metabolism in *Rheb*$^{-/-}$ hearts.** *A*, electron microscopic analysis. *Scale bar*, 2.5 μm. *B*, average of sarcomeric area to cytosolic area ratios on electron micrograph. *Open* and *closed bars* represent *Rheb*$^{+/+}$ and *Rheb*$^{-/-}$ mice, respectively. Values are expressed as the mean ± S.E. (n = 3–5 per group). *, $p < 0.05$. *C*, average number of mitochondria/cell area. Values are expressed as the mean ± S.E. (n = 3 per group). *D*, mRNA translation in *Rheb*$^{-/-}$ hearts. Heart lysates were separated on a sucrose gradient. The absorbance at 254 nm is shown as a function of gradient depth. Actively translated mRNA is associated with high molecular weight polysomes deep in the gradient.

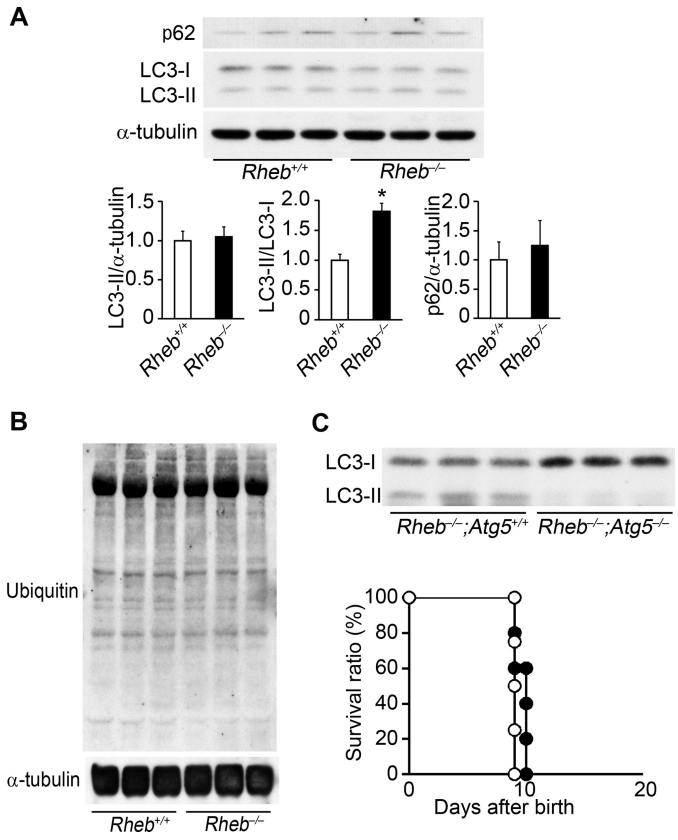

FIGURE 9. **Protein degradation systems are not involved in the cardiac phenotypes in *Rheb*$^{-/-}$ mice.** *A*, Western blot analysis of *Rheb*$^{-/-}$ hearts using anti-p62 or LC3 antibody. *Lower panels* show densitometric analysis. The average value for *Rheb*$^{+/+}$ mice was set equal to 1. Values are expressed as the mean ± S.E. (n = 3). *, $p < 0.05$. *B*, Western blot analysis of *Rheb*$^{-/-}$ hearts using anti-ubiquitin antibody. *C*, analysis of Rheb, Atg5 double knockout mice. *Upper panel* shows Western blot analysis of *Rheb*$^{-/-}$;*Atg5*$^{-/-}$ hearts using anti-LC3 antibody. *Lower panel* shows survival curve of *Rheb*$^{-/-}$;*Atg5*$^{+/+}$ and *Rheb*$^{-/-}$;*Atg5*$^{-/-}$ mice after birth. *Open* and *closed circles* represent *Rheb*$^{-/-}$;*Atg5*$^{+/+}$ (n = 4) and *Rheb*$^{-/-}$;*Atg5*$^{-/-}$ (n = 5) mice, respectively.

in the heart (Fig. 7*A*). Those also indicate that mTORC1 is involved in both proliferation and protein synthesis during early postnatal cardiac development. Although Rheb-dependent mTORC1 activation is required for cardiac hypertrophic growth at postnatal day 8, Rheb-independent mTORC1 pathway plays an important role in cardiac development at postnatal day 3 (Fig. 7*B*). The contribution of the Rheb-independent mTORC1 pathway in cardiac growth at postnatal day 8 remains to be elucidated. mTORC1 has been reported to be activated by several Rheb-independent pathways (3). Akt activation by growth factors can activate mTORC1 in a TSC1/2-independent manner by promoting the phosphorylation and dissociation of PRAS40 from mTORC1 (28, 29). In fact, we detected an increase in the phosphorylation level of PRAS40 in *Rheb*$^{-/-}$ hearts at postnatal day 3 (Fig. 6*F*). The energy status of the cell is signaled to mTORC1 through AMP-activated protein kinase 1. AMP-activated protein kinase 1 reduces mTORC1 activity by phosphorylating TSC2 (30) or directly phosphorylating Raptor (31). However, we detected no significant difference in phosphorylation level of AMP-activated protein kinase 1 between *Rheb*$^{-/-}$ and *Rheb*$^{+/+}$ mice at postnatal day 8 (data not shown). Amino acids, especially leucine, activate mTORC1 in a TSC1/2-independent manner (32). Leucine administration slightly improved the survival of *Rheb*$^{-/-}$ mice (age when all mice died; postnatal day 10 and 11 for control and leucine-treated *Rheb*$^{-/-}$ mice, respectively) (data not shown). However, we cannot exclude a possibility that the extension of survival is due to nonspecific improvement of nutritional status. The Rheb-independent mTORC1 signaling pathway in the neonatal period soon after birth remains to be investigated.

It has been reported that cardiomyocyte cell volume remains constant in rat hearts during the first 3 days of age, whereas cell number increases between days 1 and 3 after birth (33). After day 3, the number of cardiomyocytes in the heart remains relatively constant, and the volume of cardiomyocyte begins to

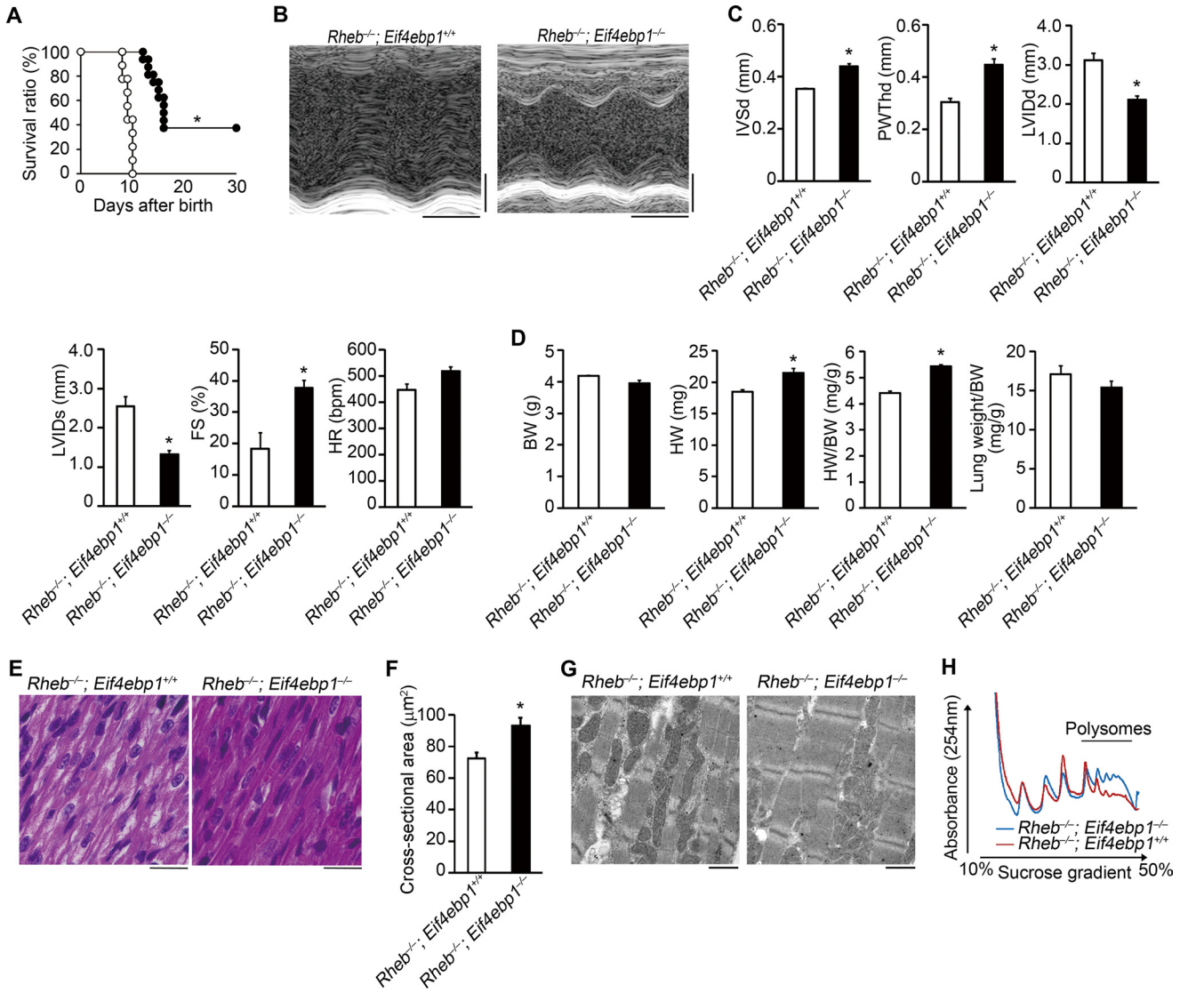

FIGURE 10. **Ablation of *Eif4ebp1* rescued the cardiac phenotypes in *Rheb*$^{-/-}$ mice.** *A*, survival ratio of *Rheb*$^{-/-}$;*Eif4ebp1*$^{-/-}$ and *Rheb*$^{-/-}$;*Eif4ebp1*$^{+/+}$ mice after birth. *Open* and *closed circles* represent *Rheb*$^{-/-}$;*Eif4ebp1*$^{+/+}$ ($n = 9$) and *Rheb*$^{-/-}$;*Eif4ebp1*$^{-/-}$ mice ($n = 16$), respectively. *, $p < 0.05$. *B*, representative M-mode echocardiographic tracings at postnatal day 8. *Scale bars*, 0.1 s and 1 mm, respectively. In *C*, *D*, and *F*, *open* and *closed bars* represent *Rheb*$^{-/-}$;*Eif4ebp1*$^{+/+}$ and *Rheb*$^{-/-}$;*Eif4ebp1*$^{-/-}$ mice, respectively, and values are expressed as the mean ± S.E. *, $p < 0.05$. *C*, echocardiographic parameters of *Rheb*$^{-/-}$;*Eif4ebp1*$^{-/-}$ ($n = 5$) and *Rheb*$^{-/-}$;*Eif4ebp1*$^{+/+}$ mice ($n = 3$) at postnatal day 8. *IVSd* indicates diastolic interventricular septum thickness; *PWThd*, diastolic left ventricular posterior wall thickness; *LVIDd*, end diastolic left ventricle internal dimension; *LVIDs*, end systolic left ventricle internal dimension; *FS*, left ventricle fractional shortening; *HR*, heart rate. *D*, physiological parameters of *Rheb*$^{-/-}$;*Eif4ebp1*$^{-/-}$ ($n = 3$) and *Rheb*$^{-/-}$;*Eif4ebp1*$^{+/+}$ mice ($n = 3$) at postnatal day 8. *BW* and *HW* indicate body weight and heart weight, respectively. *E*, hematoxylin-eosin-stained heart sections. *Scale bar*, 20 μm. *F*, cross-sectional area of cardiomyocytes ($n = 3$). *G*, electron microscopic analysis. *Scale bar*, 1 μm. *H*, mRNA translation. Heart lysates were separated on a sucrose gradient. The absorbance at 254 nm is shown as a function of gradient depth.

increase. Thus, it is possible that the Rheb-mTORC1 signaling pathway is necessary for heart development after transition of cardiomyocytes from proliferation to hypertrophic growth after early postnatal period. In this study, the cardiomyocyte surface area in the heart was dramatically increased between postnatal days 5 and 8 in *Rheb*$^{+/+}$ mice, whereas it remained constant during this period in *Rheb*$^{-/-}$ mice.

There may be several possible mechanisms underlying the development of dilated cardiomyopathy in *Rheb*$^{-/-}$ mice. Recently, it has been reported that ablation of *Mtor* in the adult mouse myocardium results in fatal, dilated cardiomyopathy that is characterized by an increase in apoptosis, induction of autophagy, altered mitochondrial structure, and accumulation of 4E-BP1 (34). Ablation of *Eif4ebp1* improved cardiac function and survival with a decreased level of apoptosis in *Mtor*$^{-/-}$ mice, whereas overexpression of a non-phosphorylatable form of 4E-BP1 in isolated cardiomyocytes induced apoptosis. The authors suggested that increased apoptosis might be a cause for the development of cardiomyopathy in *Mtor*$^{-/-}$ mice. However, we did not observe an increase in apoptosis in *Rheb*$^{-/-}$ mice. One possible explanation for the discrepancy between our results and those obtained with the use of *Mtor*$^{-/-}$ mice may be due to the fact that mTOR deletions affect both mTOR complexes mTORC1 and -2. Another explanation is that the involvement of mTOR in apoptosis may be mediated through a Rheb-independent signaling pathway. It is also possible that the role of mTORC1 may be different between adulthood and neonatal periods.

It has been reported that mTORC1 suppresses autophagy (10). However, we did not detect an increase in autophagic activity in *Rheb*$^{-/-}$ mice, and ablation of *Atg5* had no effect on survival of *Rheb*$^{-/-}$ mice, suggesting that autophagy was not related to the premature death of *Rheb*$^{-/-}$ mice. Rheb-dependent mTORC1 activation might not be a major signaling pathway to regulate autophagy in the heart.

Activation of mTORC1 stimulates mRNA translation via its downstream substrates 4E-BP1 and S6 kinase (9). In this study, we found that *Rheb* ablation led to an increase in the nonphosphorylated form of 4E-BP1, a decrease in S6 kinase activity and reduction in translation. The rescue experiment using *Rheb*$^{-/-}$;*Eif4ebp1*$^{-/-}$ mice indicates that the mTORC1–4E-BP1 axis plays an important role in the maintenance of cardiac function and structure during the neonatal period after transition from proliferation to hypertrophic growth. The development of dilated cardiomyopathy in *Rheb*$^{-/-}$ mice appears to result from the lack of cardiac hypertrophic growth due to the reduction in translation. In this experiment, ablation of *Eif4ebp1* was able to improve survival of *Rheb*$^{-/-}$ mice but failed to accomplish complete rescue of survival. Because we observed chamber dilatation in dead *Rheb*$^{-/-}$;*Eif4ebp1*$^{-/-}$ mice, heart failure appears to be the cause of death in these animals (data not shown). We did not identify the molecular mechanism underlying the premature death in *Rheb*$^{-/-}$;*Eif4ebp1*$^{-/-}$ mice. Some pathway other than the mTORC1–4E-BP1 signaling pathway such as mTORC1-S6 kinase and mTORC1–4E-BP2 may be involved in the premature death in *Rheb*$^{-/-}$;*Eif4ebp1*$^{-/-}$ mice.

In conclusion, the Rheb signaling pathway is essential for normal heart development from postnatal day 5. In this period, the Rheb-mTORC1–4E-BP1 signaling cascade plays a pivotal role in mRNA translation and protein synthesis and thereby cardiac hypertrophic growth.

Acknowledgments—We thank professor Noboru Mizushima (Tokyo Medical and Dental University) for a gift of Atg5$^{flox/flox}$ *mice and Kana Takada and Sachie Koyama for technical assistance.*

REFERENCES

1. Ahuja, P., Sdek, P., and MacLellan, W. R. (2007) Cardiac myocyte cell cycle control in development, disease, and regeneration. *Physiol. Rev.* **87,** 521–544
2. Shiojima, I., and Walsh, K. (2006) Regulation of cardiac growth and coronary angiogenesis by the Akt/PKB signaling pathway. *Genes Dev.* **20,** 3347–3365
3. Laplante, M., and Sabatini, D. (2009) mTOR signaling at a glance. *J. Cell Sci.* **122,** 3589–3594
4. Gromov, P. S., Madsen, P., Tomerup, N., and Celis, J. E. (1995) A novel approach for expression cloning of small GTPases: identification, tissue distribution and chromosome mapping of the human homolog of rheb. *FEBS Lett.* **377,** 221–226
5. Yamagata, K., Sanders, L. K., Kaufmann, W. E., Yee, W., Barnes, C. A., Nathans, D., and Worley, P. F. (1994) rheb, a growth factor- and synaptic activity-regulated gene, encodes a novel Ras-related protein. *J. Biol. Chem.* **269,** 16333–16339
6. Inoki, K., Li, Y., Xu, T., and Guan, K. L. (2003) Rheb GTPase is a direct target of TSC2 GAP activity and regulates mTOR signaling. *Genes Dev.* **17,** 1829–1834
7. Gingras, A. C., Raught, B., and Sonenberg, N. (2001) Regulation of translation initiation by FRAP/mTOR. *Genes Dev.* **15,** 807–826
8. Richter, J. D., and Sonenberg, N. (2005) Regulation of cap-dependent translation by eIF4E inhibitory proteins. *Nature* **433,** 477–480
9. Magnuson, B., Ekim, B., and Fingar, D. C. (2012) Regulation and function of ribosomal protein S6 kinase (S6K) within mTOR signalling networks. *Biochem. J.* **441,** 1–21
10. Ravikumar, B., Vacher, C., Berger, Z., Davies, J. E., Luo, S., Oroz, L. G., Scaravilli, F., Easton, D. F., Duden, R., O'Kane, C. J., and Rubinsztein, D. C. (2004) Inhibition of mTOR induces autophagy and reduces toxicity of polyglutamine expansions in fly and mouse models of Huntington disease. *Nat. Genet.* **36,** 585–595
11. Kim, J., Kundu, M., Viollet, B., and Guan, K. L. (2011) AMPK and mTOR regulate autophagy through direct phosphorylation of Ulk1. *Nat. Cell Biol.* **13,** 132–141
12. Goorden, S. M., Hoogeveen-Westerveld, M., Cheng, C., van Woerden, G. M., Mozaffari, M., Post, L., Duckers, H. J., Nellist, M., and Elgersma, Y. (2011) Rheb Is essential for murine development. *Mol. Cell. Biol.* **31,** 1672–1678
13. Zou, J., Zhou, L., Du, X. X., Ji, Y., Xu, J., Tian, J., Jiang, W., Zou, Y., Yu, S., Gan, L., Luo, M., Yang, Q., Cui, Y., Yang, W., Xia, X., Chen, M., Zhao, X., Shen, Y., Chen, P. Y., Worley, P. F., and Xiao, B. (2011) Rheb1 is required for mTORC1 and myelination in postnatal brain development. *Dev. Cell* **20,** 97–108
14. Wang, Y., Huang, B. P., Luciani, D. S., Wang, X., Johnson, J. D., and Proud, C. G. (2008) Rheb activates protein synthesis and growth in adult rat ventricular cardiomyocytes. *J. Mol. Cell Cardiol.* **45,** 812–820
15. Sciarretta, S., Zhai, P., Shao, D., Maejima, Y., Robbins, J., Volpe, M., Condorelli, G., and Sadoshima, J. (2012) Rheb is a critical regulator of autophagy during myocardial ischemia: Pathophysiological implications in obesity and metabolic syndrome. *Circulation* **125,** 1134–1146
16. Liu, P., Jenkins, N. A., and Copeland, N. G. (2003) A highly efficient recombineering-based method for generating conditional knockout mutations. *Genome Res.* **13,** 476–484
17. Nishida, K., Yamaguchi, O., Hirotani, S., Hikoso, S., Higuchi, Y., Watanabe, T., Takeda, T., Osuka, S., Morita, T., Kondoh, G., Uno, Y., Kashiwase, K., Taniike, M., Nakai, A., Matsumura, Y., Miyazaki, J., Sudo, T., Hongo, K., Kusakari, Y., Kurihara, S., Chien, K. R., Takeda, J., Hori, M., and Otsu, K. (2004) p38α mitogen-activated protein kinase plays a critical role in cardiomyocyte survival but not in cardiac hypertrophic growth in response to pressure overload. *Mol. Cell. Biol.* **24,** 10611–10620
18. Tsukiyama-Kohara, K., Poulin, F., Kohara, M., DeMaria, C. T., Cheng, A., Wu, Z., Gingras, A. C., Katsume, A., Elchebly, M., Spiegelman, B. M., Harper, M. E., Tremblay, M. L., and Sonenberg, N. (2001) Adipose tissue reduction in mice lacking the translational inhibitor 4E-BP1. *Nat. Med.* **7,** 1128–1132
19. Hara, T., Nakamura, K., Matsui, M., Yamamoto, A., Nakahara, Y., Suzuki-Migishima, R., Yokoyama, M., Mishima, K., Saito, I., Okano, H., and Mizushima, N. (2006) Suppression of basal autophagy in neural cells causes neurodegenerative disease in mice. *Nature* **441,** 885–889
20. Hikoso, S., Yamaguchi, O., Higuchi, Y., Hirotani, S., Takeda, T., Kashiwase, K., Watanabe, T., Taniike, M., Tsujimoto, I., Asahi, M., Matsumura, Y., Nishida, K., Nakajima, H., Akira, S., Hori, M., and Otsu, K. (2004) Pressure overload induces cardiac dysfunction and dilation in signal transducer and activator of transcription 6-deficient mice. *Circulation* **110,** 2631–2637
21. Nakai, A., Yamaguchi, O., Takeda, T., Higuchi, Y., Hikoso, S., Taniike, M., Omiya, S., Mizote, I., Matsumura, Y., Asahi, M., Nishida, K., Hori, M., Mizushima, N., and Otsu, K. (2007) The role of autophagy in cardiomyocytes in the basal state and in response to hemodynamic stress. *Nat. Med.* **13,** 619–624
22. Dowling, R. J., Zakikhani, M., Fantus, I. G., Pollak, M., and Sonenberg, N. (2007) Metformin inhibits mammalian target of rapamycin-dependent translation initiation in breast cancer cells. *Cancer Res.* **67,** 10804–10812
23. Lyons, G. E., Schiaffino, S., Sassoon, D., Barton, P., and Buckingham, M. (1990) Developmental regulation of myosin gene expression in mouse cardiac muscle. *J. Cell Biol.* **111,** 2427–2436
24. Dowling, R. J., Topisirovic, I., Alain, T., Bidinosti, M., Fonseca, B. D., Petroulakis, E., Wang, X., Larsson, O., Selvaraj, A., Liu, Y., Kozma, S. C.,

Thomas, G., and Sonenberg, N. (2010) mTORC1-mediated cell proliferation, but not cell growth, controlled by the 4E-BPs. *Science* **328,** 1172–1176

25. Koritzinsky, M., Magagnin, M. G., van den Beucken, T., Seigneuric, R., Savelkouls, K., Dostie, J., Pyronnet, S., Kaufman, R. J., Weppler, S. A., Voncken, J. W., Lambin, P., Koumenis, C., Sonenberg, N., and Wouters, B. G. (2006) Gene expression during acute and prolonged hypoxia is regulated by distinct mechanisms of translational control. *EMBO J.* **25,** 1114–1125
26. McMullen, J. R., Shioi, T., Zhang, L., Tarnavski, O., Sherwood, M. C., Dorfman, A. L., Longnus, S., Pende, M., Martin, K. A., Blenis, J., Thomas, G., and Izumo, S. (2004) Deletion of ribosomal S6 kinases does not attenuate pathological, physiological, or insulin-like growth factor 1 receptor-phosphoinositide 3-kinase-induced cardiac hypertrophy. *Mol. Cell. Biol.* **24,** 6231–6240
27. Yuan, J., Shan, Y., Chen, X., Tang, W., Luo, K., Ni, J., Wan, B., and Yu, L. (2005) Identification and characterization of RHEBL1, a novel member of Ras family, which activates transcriptional activities of NF-κB. *Mol. Biol. Rep.* **32,** 205–214
28. Sancak, Y., Thoreen, C. C., Peterson, T. R., Lindquist, R. A., Kang, S. A., Spooner, E., Carr, S. A., and Sabatini, D. M. (2007) PRAS40 is an insulin-regulated inhibitor of the mTORC1 protein kinase. *Mol. Cell* **25,** 903–915
29. Vander Haar, E., Lee, S. I., Bandhakavi, S., Griffin, T. J., and Kim, D. H. (2007) Insulin signalling to mTOR mediated by the Akt/PKB substrate PRAS40. *Nat. Cell Biol.* **9,** 316–323
30. Inoki, K., Zhu, T., and Guan, K. L. (2003) TSC2 mediates cellular energy response to control cell growth and survival. *Cell* **115,** 577–590
31. Gwinn, D. M., Shackelford, D. B., Egan, D. F., Mihaylova, M. M., Mery, A., Vasquez, D. S., Turk, B. E., and Shaw, R. J. (2008) AMPK phosphorylation of raptor mediates a metabolic checkpoint. *Mol. Cell* **30,** 214–226
32. Nobukuni, T., Joaquin, M., Roccio, M., Dann, S. G., Kim, S. Y., Gulati, P., Byfield, M. P., Backer, J. M., Natt, F., Bos, J. L., Zwartkruis, F. J., and Thomas, G. (2005) Amino acids mediate mTOR/raptor signaling through activation of class 3 phosphatidylinositol 3OH-kinase. *Proc. Natl. Acad. Sci. U.S.A.* **102,** 14238–14243
33. Li, F., Wang, X., Capasso, J. M., and Gerdes, A. M. (1996) Rapid transition of cardiac myocytes from hyperplasia to hypertrophy during postnatal development. *J. Mol. Cell. Cardiol.* **28,** 1737–1746
34. Zhang, D., Contu, R., Latronico, M. V., Zhang, J., Zhang, J. L., Rizzi, R., Catalucci, D., Miyamoto, S., Huang, K., Ceci, M., Gu, Y., Dalton, N. D., Peterson, K. L., Guan, K. L., Brown, J. H., Chen, J., Sonenberg, N., and Condorelli, G. (2010) MTORC1 regulates cardiac function and myocyte survival through 4E-BP1 inhibition in mice. *J. Clin. Invest.* **120,** 2805–2816